APPLIED PHYSICS

Magnetic flux tailoring through Lenz lenses for ultrasmall samples: A new pathway to high-pressure nuclear magnetic resonance

Thomas Meier,[1]* Nan Wang,[2] Dario Mager,[2] Jan G. Korvink,[2]
Sylvain Petitgirard,[1] Leonid Dubrovinsky[1]

A new pathway to nuclear magnetic resonance (NMR) spectroscopy for picoliter-sized samples (including those kept in harsh and extreme environments, particularly in diamond anvil cells) is introduced, using inductively coupled broadband passive electromagnetic lenses, to locally amplify the magnetic field at the isolated sample, leading to an increase in sensitivity. The lenses are adopted for the geometrical restrictions imposed by a toroidal diamond indenter cell and yield signal-to-noise ratios at pressures as high as 72 GPa at initial sample volumes of only 230 pl. The corresponding levels of detection are found to be up to four orders of magnitude lower compared to formerly used solenoidal microcoils. Two-dimensional nutation experiments on long-chained alkanes, C_nH_{2n+2} (n = 16 to 24), as well as homonuclear correlation spectroscopy on thymine, $C_5H_6N_2O_2$, were used to demonstrate the feasibility of this approach for higher-dimensional NMR experiments, with a spectral resolution of at least 2 parts per million. This approach opens up the field of ultrahigh-pressure sciences to one of the most versatile spectroscopic methods available in a pressure range unprecedented up to now.

INTRODUCTION

Nuclear magnetic resonance (NMR) spectroscopy is by far the most widespread analytical method in modern life science. Biology, chemistry, and medicine are benefiting from the ability of the NMR to locally yield valuable structural, electronic, and dynamical information; it is used by an ever-growing community spanning almost all the natural sciences (1–3). Because of the development of in vivo magnetic resonance imaging (4, 5) and because of its singular analytical role in the investigation of proteins (6–8), NMR has become an integral part in these research fields.

Besides its widespread use, there are some research branches where a broader application of NMR seems unfeasible, for example, in high-pressure chemistry and physics, or mineral physics, where harsh experimental conditions such as high pressure and high temperature are mandatory. Nevertheless, NMR under these extreme conditions will certainly have a great impact generally on natural sciences and particularly on modern high-pressure chemistry and geosciences, where the application of NMR is so far mostly restricted to ex situ measurements on recovered samples (9, 10). At the same time, application of NMR could help in resolving these fundamental problems, for example, as birth of life on our planet: It is believed that the first signs of life on Earth developed in the considerable depths of the proto-ocean of the hadean era under high-pressure conditions (11–13). Thus, NMR studies of proteins and their stability at appropriate pressure-temperature conditions may provide answers to the most important question of contemporary science.

The main obstacle against the application of high-pressure NMR lies in its inherently low sensitivity and the requirement that the radio frequency (RF) antenna must be very close to the sample, ensuring a good filling factor of the resonator (14). In high pressure–generating vessels, that is, in diamond anvil cells (DACs), typical available sample spaces

are less than 1 nl and are also tightly enclosed by two diamond anvils and a metallic gasket; thus, the use of in situ NMR experiments was widely considered an impossibility for several decades.

Nonetheless, several research groups were able to implement NMR in DACs at pressures up to 10 GPa (1 GPa = 10,000 bar), and a more complete overview of the development of high-pressure NMR techniques in DACs is presented elsewhere (15). These previous setups suffered from low sensitivities and therefore were only applicable to systems rich in "high-γ_n" nuclei, such as hydrogen or fluorine, which provide the highest signal-to-noise ratios (SNRs) and thus the best sensitivity in an NMR experiment. A turning point was the implementation of microcoils in NMR research. As demonstrated by Peck et al. (16), reducing the dimensions of the RF resonators will result in significantly improved sensitivity, as well as much higher spectral resolution (17, 18), and allows wide-line excitations of broad NMR signals (19).

In 2009, Suzuki et al. (20) introduced the idea of placing a minuscule microcoil—typically 400 to 500 μm in diameter and 100 to 250 μm in height—directly in the sample chamber between the anvil vise, and it has been shown that this technique was superior to the previous attempts in terms of spin sensitivities (21, 22) and reachable pressures of up to 30 GPa (23).

The bold approach came with some drawbacks. The extremely fragile microcoils are typically made from very thin insulated gold or copper wire, and become exceedingly difficult to manufacture and handle if a further miniaturization is needed to reach pressures above 10 GPa (24) with an imposed empirical pressure limit of about 10 to 15 GPa. In any case, preparation of DACs for high-pressure NMR measurements with microcoils is rather an art than a science, which limits the application of the method.

At present, the most pressing scientific questions in high-pressure chemistry and the geosciences concern topics such as high-pressure phase transitions toward new exotic materials (25, 26), coordination changes or spin transitions of Earth's mantle materials (27–29), or metallizations or even transitions into a superconducting state of diatomic molecules such as hydrogen (30–33); these all occur predominantly at much higher pressures close to the megabar regime (1 Mbar = 100 GPa)

[1]Bayerisches Geoinstitut, Bayreuth University, Universitätsstraße 30, 95447 Bayreuth, Germany. [2]Institute of Microstructure Technology, Karlsruhe Institute of Technology, Hermann-von-Helmholtz-Platz 1, 76344 Eggenstein-Leopoldshafen, Germany.
*Corresponding author. Email: thomas.meier@uni-bayreuth.de

or even beyond. Therefore, to implement in situ NMR measurements at these extreme pressures, new RF resonators must be developed, which enable a successful detection of the NMR signal from within the pressure chamber, yielding high sensitivities throughout the whole experiment.

RESULTS

Sample spectra and sensitivity

A possible solution was introduced using magnetic flux tailoring Lenz lenses, which were recognized recently to locally amplify the magnetic field at a given region of interest by Schoenmaker et al. (34) and in more detail by Spengler et al. (35). This magnetic lens consists of a single current-carrying track, made either directly as small wire segments of some micrometer thickness or using a solid sheet of metal foil. In the latter case, the single current-carrying track is defined by the limiting RF penetration depth δ, the skin depth, which depends on the conductivity of the material and the frequency of the current. In general, the Lenz lens is a flux transformer. Its outer winding collects the flux from a larger area, which, in response, builds up a current in its continuous perimeter conductor, and its inner anti-winding deposits this flux over a very small area. The Lenz law ensures that the flux in the region between the anti-winding and the winding will be zero so that the flux is only deposited over the inner region of interest. Because its conductor length is very small, the effective resistance is small, too, due to the microscopic Ohm's law. Furthermore, because its effective capacitance is negligible due to the small length of the gap, its resonance is very high, way beyond the NMR resonance. As a result, it appears as a pure inductance—following the outer coil without lag—and is inductively coupled to the outer coil through its mutual inductance, requiring some additional matching but hardly any detuning of the outer coil. As a result, it almost perfectly increases SNR [by reciprocity (36–38) because now all the current is used to generate field in only a very small region] without significantly reducing the quality factor of the resonator Q.

It could be shown that these resonators are capable of focusing the total magnetic field of the resonator at its center, leading to a locally enhanced sensitivity. Similar approaches to locally amplify the receiving sensitivity of a given NMR resonator structure were recently realized by microfabricated inserts for magic angle coil spinning (39, 40) for mass limited samples.

This study will demonstrate that inductively coupled Lenz lenses can be used in a DAC (see Fig. 1 for a schematic overview of the setup used.) ^{1}H NMR spectra obtained from paraffin up to 72 GPa show the applicability of the lenses in high-pressure NMR research. Furthermore, using numerical finite element simulations, it is revealed that application of a quasi–two-dimensional (2D) resonator is preferable to the bigger and more fragile solenoidal coils placed within the high-pressure chamber, which have been used before.

Finally, 2D nutation and ^{1}H-^{1}H COSY (correlation spectroscopy) experiments demonstrate that this setup can even be used for higher-dimensional NMR experiments. Preparation of the pressure cell and the RF resonator is described in Materials and Methods.

To compare sensitivities and performances under pressure for different resonator types, it is instructive to define the limit of detection in the time domain (LOD_t) as the minimum necessary number of spins that resonate within a bandwidth of 1 Hz, yielding an SNR of unity (41)

$$LOD_t = \frac{N_{spins}}{SNR_t \cdot \sqrt{\Delta f}} \qquad (1)$$

where N_{spins} denotes the number of spins that contribute to the signal, SNR_t is the SNR acquired in time domain, and Δf is the receiver bandwidth. Assuming that the sample chamber is filled completely with a liquid paraffin oil sample, the number of resonant spins can be gauged to be about 1.7×10^{16}. The effect of the Lenz lens on the sensitivity at ambient pressure in the DAC is shown in Fig. 2A. The use of the lens strongly enhances the SNR, and thus, LOD_t is compared to the same arrangement measured without a lens. The bad performance without the lens partly originates in very poor filling factors of the outer excitation coil ($\eta \approx 3 \times 10^{-4}$) and in B_1 field inhomogeneities at the sample. The "lense-less" arrangement is similar to previous attempts to perform high-pressure NMR in DACs, yielding comparable sensitivities (42).

The deformation of the lens under axial pressure is shown in Fig. 2B. Its overall shape remains stable at pressures up to about 7 GPa, after which the gold begins to deform up to about 20 GPa. A short circuit, which would occur if the 30-μm slit is closed, did not occur, possibly because some amount of the insulating Al_2O_3 layer between rhenium gasket and Lenz lens (see the Supplementary Materials) had been squeezed into the slit, preventing a complete closure of the lens structure. The inner hole diameter was found to be increased by about 5% at 72 GPa compared to ambient pressure, together with a sliding of the hole away from the pressure center by about 15 μm, originating from small misalignments of the anvil tips. The average RF field strength $\langle B_1 \rangle$ produced by the lenses was found to be almost constant, as indicated by the obtained values from 2D nutation experiments (see Table 1). In principle, B_1 should scale with the inverse inner diameter of the lens. Nevertheless, this effect is most likely masked by the presence of the metallic rhenium gasket, which is in close proximity to the lens, and certainly also contributes somewhat to the total $\langle B_1 \rangle$ field strength and homogeneity in the sample cavity.

Figure 2C summarizes recorded single-scan ^{1}H NMR spectra of paraffin, and Fig. 2D shows the evolution of the full width at half maximum (FWHM) linewidths. In the liquid phase, FWHM was found to
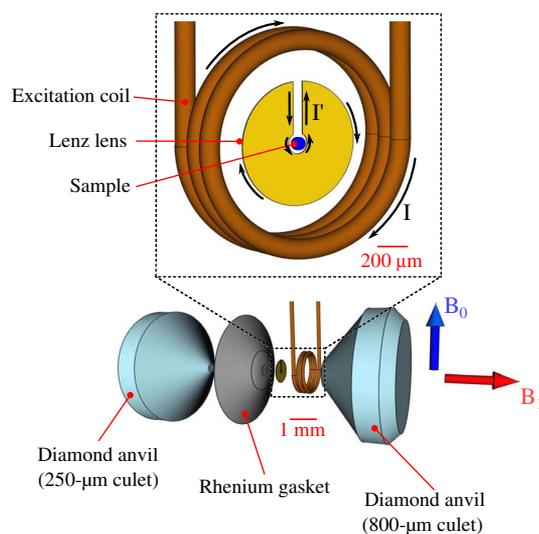
Fig. 1. Schematic explosion diagram of the resonator setup and the anvil/gasket arrangement. The blue and red arrows denote the directions of the external magnetic field B_0 and the RF magnetic field B_1, respectively, generated by the excitation coil and the lens, which is compressed between the rhenium gasket and the 800-μm culeted diamond anvil. The enlarged picture shows the RF arrangement of the excitation coil with the Lenz lens. Black arrows denote the directions of the high-frequency current.

increase from 5 parts per million (ppm) at ambient pressure (10^{-4} GPa) to about 15 ppm at 7 GPa. At higher pressures, above the amorphization pressure of paraffin oil (43–45) at about 10 to 12 GPa, the linewidths begin to increase, exponentially reaching 23 ppm at 72 GPa. This effect is consistent with previous investigations of pressure gradients in the sample hole using paraffin oil as a pressure medium [see figure 3 from the studies of Yamauchi et al. (19) and Meier and Haase (23) or figure 19 from the study of Meier (15)].

The relatively narrow proton spectra indicate a nonvanishing mobility of the methylene and methyl groups in paraffin. Similar dynamic effects could be observed in molecular hydrogen in guest matrices under elevated pressures (46–48). To investigate this effect further, spin-lattice (T_1) and spin-spin (T_2) relaxation measurements would illuminate the contribution of rotational and diffusional motion of the ^1H nuclei. The appearance of the observed doublet at 72 GPa will be addressed in the next section. The sensitivity and detection limits (LOD) were calculated using Eq. 1 and were found to be almost constant, with an increase from 6×10^{11} spins/$\sqrt{Hz}$ at ambient conditions to 1.5×10^{12} spins/$\sqrt{Hz}$ at 72 GPa (see Table 1).

Figure 3 compares the resulting LOD_t of the Lenz lens resonator with three experimental runs using solenoidal microcoils in the sample chamber, reaching maximal pressures of 10 GPa (49), 20 GPa (22), and 30 GPa (23). In these experiments, the microcoils range between 300 and 500 μm in diameter and 100 and 250 μm in height, tightly fitting

into the initial sample volume. Evidently, the sensitivity of microcoils exhibits a strong pressure dependence, culminating in serious degradations of up to two orders of magnitude compared to their initial performances at ambient conditions.

Strikingly, the LOD of the Lenz lens setup were found to be not only several orders of magnitude lower (and thus more sensitive) but also very stable, with small sensitivity losses of about 2% per GPa throughout the whole pressure run. The significantly better performance partially originates from the fact that, in flat solenoidal microcoils, half of the magnetic field is dissipated at the outside the coil, whereas the region within the microcoil also exhibits large B_1 field inhomogeneities (50), which will be eventually amplified by mechanical deformations because the sample cavity shrinks under compression and the microcoils will be squeezed between the anvils.

The RF magnetic field generated by the Lenz lenses, on the other hand, is focused within the part of its inner diameter and a limited space above or below it, leading to a much higher concentration and homogeneity across the DAC sample chamber. To this end, one defines the effective sample volume $V_{eff} = \alpha V_0$ as the total volume V_0 reduced by a factor α, which is between 0 and 1, and as the volume in which the generated RF magnetic field B_1 is within 10 to 20% of the maximum value at the center of the coil. The obtainable SNR in an NMR experiment will be directly proportional to V_{eff} because it determines the observable fraction of the sample placed within a given resonator. Therefore, the
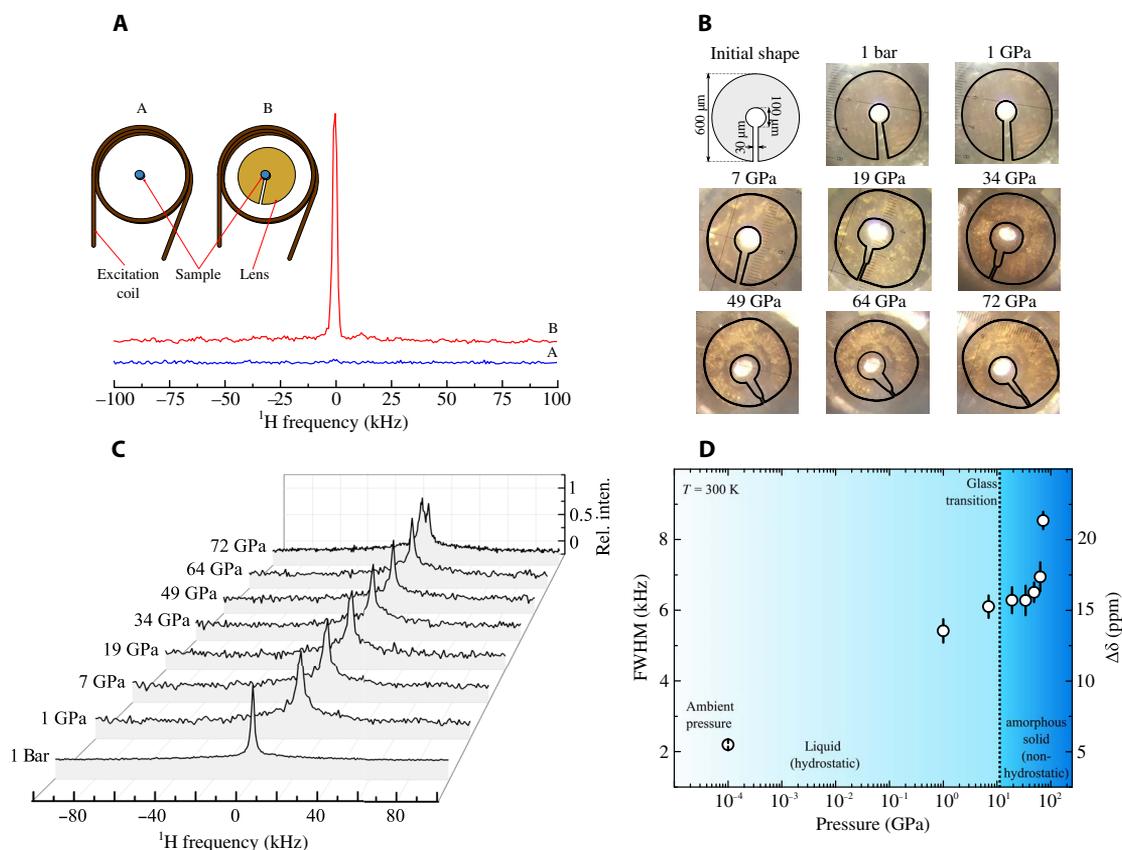
Fig. 2. Sensitivity and stability tests of the Lenz lens resonator setup in a DAC. (**A**) Proton spectra of paraffin at ambient pressure with and without the use of a Lenz lens. (**B**) Photographs of different deformation states of the lens under pressure. Black contours are guide to the eye. (**C**) Recorded ^1H NMR spectra. At ambient conditions, 100 scans were accumulated, whereas at higher pressures, only single-shot spectra after a single π/2 pulse were recorded. (**D**) Pressure dependence of the FWHM linewidths. The dotted line denotes the crystallization pressure at ambient temperature, and the shaded areas denote the liquid and amorphous phases of paraffin. The glass transition pressure was obtained from other methods.

sensitivity of every setup is closely related to the strength and homogeneity of the generated B_1 field.

Thus, to further elucidate this problem, we performed numerical simulations using the FEMM software package to simulate RF magnetic field maps for both resonator setups. The results of the simulations comparing the initial magnetic fields before pressurization with a significantly deformed arrangement are shown in fig. S5.

In accordance with similar calculations from van Bentum et al. (50), the B_1 field map in the x-z plane of a flat microcoil, with a length-to-diameter ratio of less than unity, the magnetic field is rather inhomogeneously distributed, with the highest magnetic fields close to the respective windings. The effective observable sample volume, V_{eff}, with a B_1 homogeneity within 20% of the central field accounts to about 1.7 nl, which is about 14% of the total available sample space, and stores only 6% of the total magnetic field energy of the microcoil.

Moreover, as indicated by the "deformed resonator," the B_1 field homogeneity greatly suffers from an irregular arrangement of the current-carrying wire segments of the microcoil. This deformed state typically arises already at relatively low pressures. Depending on the choice of gasket materials and the geometry of the sample cavity, a collapse can occur at relatively low pressures of some gigapascals, which will lead to significant deformations of the interior of the cavity including the placed microcoils. In this particular case, V_{eff} drops to a $1/20$th of a percent because of significant B_1 field inhomogeneities while at the same time storing only about 0.003% of the total magnetic field energy. In addition, at these compressions, the risk for coil gasket or interturn short circuits increases rapidly (51), rendering the application of microcoils in DACs increasingly unreliable above 10 GPa. This effect becomes even more evident if the actual microcoil geometries used in the corresponding experiments are considered. Meissner (52) used a microcoil made from $d = 10\,\mu m$ insulated (plus 5 μm insulation layer) copper wire, consisting of $n = 10$ turns. The total height of the coil can be gauged (16), using $h \approx 1.5\,Nd$, to be 225 μm, which is already about 50 μm higher than the initial sample chamber drilled into the CuBe gasket used. For the study reaching 20 GPa, Meier et al. (22) used microcoils consisting of four to five turns with insulated copper wire of 23 μm thickness (140 to 170 μm total height). As can be seen, the pressure-induced degradation in LOD_t is reduced by about half an order of magnitude compared to the pressure run reaching only 10 GPa. Finally, in the experiments reaching 30 GPa, microcoils of only 70 μm could be used with considerably reduced sample chambers and hybrid gasket materials. Evidently, the LOD could be improved considerably by at least one order of magnitude but still did not permit very high sensitivity NMR above this pressure.

In the case of the Lenz lenses, on the other hand, the RF B_1 field appears to be rather homogeneous more than at least 40 to 50% of the total sample cavity, storing about 30% of the magnetic field energy. Strikingly, under compression, the situation does not deteriorate significantly, and both the stored energy ($\approx 35\%$) and V_{eff} ($\approx 47\%$) remain almost constant. The B_1 field strengths of the lens resonators found in the simulations compare well with the actual field strengths found via nutation experiments (see Table 1), which is further evidence of the applicability of this approach.

Another comparison would be noteworthy at this point. Pravica and Silvera (53, 54) introduced a remarkably similar setup using a single-loop cover inductor—directly connected to the spectrometer—which is in electrical contact to a split gasket. The split in the rhenium gasket was introduced after preindentation and filled with coarse diamond and NaCl powder. With that setup, ^1H NMR spectra of molecular hydrogen could be recorded at pressures as high as 12.8 GPa. Judging from the reported signals in time domain at 20 K, SNR values of about 10 could be realized after 1500 scans were accumulated. That would subsequently lead to LODs vastly higher, and thus less sensitive, compared to the Lenz lens resonators. Several possible reasons could be considered as the origin of this different performance. First, the homebuilt NMR spectrometer was blanked out for about 10 μs before data acquisition, leading to a significant loss of signal intensity given the presumably short spin-spin relaxation time of H_2. Furthermore, the gasket resonator is likely to have a very low quality factor, partly because the resistivity of rhenium metal is almost one order of magnitude higher compared to gold or copper,

Table 1. Summary of performance data using an inductively coupled Lenz lens resonator. The average pressure, p, was obtained at the center of the 250-μm culeted diamond anvil. The 90° pulse lengths, $t_{\pi/2}$, were obtained by nutation experiments at 1-W pulse power and used to estimate the average RF magnetic field strengths $\langle B_1 \rangle$. LOD_t was estimated given the obtained time-domain SNR, SNR_t, a number of about 1.7×10^{16} hydrogen nuclei in the sample cavity, and a receiver bandwidth of 2 MHz at all measurements.

p (GPa)	$t_{\pi/2}$ (μs)	$\langle B_1 \rangle$ (mT)	SNR_t	LOD_t (spins/$\sqrt{Hz}$)
10^{-4}	2.4	2.5	19	6×10^{11}
1	2.1	3.0	18.2	7×10^{11}
7	1.9	3.1	16.5	7.3×10^{11}
19	2.5	2.3	14.2	8.5×10^{11}
34	2.2	2.7	15	8×10^{11}
49	1.8	3.3	10	1.2×10^{12}
64	2.2	2.7	7	1.7×10^{12}
72	2.3	2.6	8	1.5×10^{12}
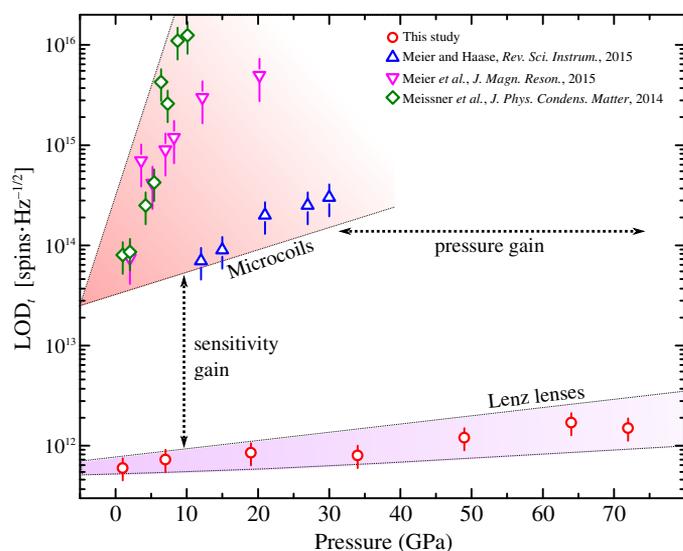
Fig. 3. LOD_t at increasing pressures obtained from microcoil experiments and from Lenz lenses. The obtained gains in sensitivity and reachable pressures are indicated by black arrows.

leading to significantly increased noise levels. Furthermore, the slit in the rhenium gasket can be considered as a capacitance close to the inductive inner loop of the gasket resonator. The dielectric of this capacitor, a mixture of diamond powder and NaCl, is known to exhibit ionic conductivity under high pressures and strain (55–57), leading to a breakdown of the electric field of capacitors into small steps of electric potential. Furthermore, as both anions and cations become mobile under pressure, imposed ionic motion will lead to a considerable increase in temperature through dissipation, leading to increased noise levels as well.

That effect will certainly diminish the advantage of proximity of the resonator to the sample cavity. Furthermore, because the gasket resonator most likely has a resonance frequency, which will be far off the NMR resonance frequency, the gasket resonator works as a purely lossy inductance in its low resonance flat region. Now, as the single-turn copper cover inductor couples with the rhenium gasket resonator, it will also turn into a lossy resonator, leading to a significantly reduced sensitivity at higher pressure than about 15 to 20 GPa.

2D NMR spectroscopy under pressure

Up to this point, 2D NMR spectroscopy has only rarely been used in DACs at pressures exceeding some few gigapascals. The most obvious reason for this reluctance to perform NMR measurements in several dimensions lies in the significant increase in total data acquisition time, an effect that becomes even more severe if the sensitivity of the resonator, and thus its SNR, is rather poor in one dimension. Given the significant increase in LOD and the corresponding decrease in measurement time when Lenz lenses are used, we performed 2D nutation experiments and homonuclear COSY (^{1}H-^{1}H COSY) in pressure cells up to 64 GPa.

In a 2D nutation experiment, the indirect time dimension is defined by an incremented RF pulse length. This method was widely used for investigations of powder patterns of quadrupolar (nuclear spin $I > 1/2$) systems, where the changing RF excitation conditions lead to a possible extraction of quadrupole frequencies and asymmetry parameters, although the complete NMR spectrum is impossible to excite with a single RF pulse in 1D (58–61).

Figure 4 summarizes obtained data from 2D nutation experiments performed on paraffin in a pressure range of 8 to 64 GPa. At lower pressures ($p \leq 8$ GPa), the intense NMR signal could be attributed to the methylene groups of the long-chained paraffin molecules. Signals from the end-chain methyl groups were not observed as distinct signals, either because of signal overlap with the CH_2 group signals or because of the low density of these spectroscopic species. However, even at low pressures such as 8 GPa, a distinct second NMR signal could be found at slightly lower nutation frequencies, which almost completely overlapped with the dominant CH_2 signal in the 1D NMR spectra shown in Fig. 2C. This additional signal could possibly be associated to the formation of methine groups. Because pressure was increased (see Fig. 4B), the signal intensity of CH_2 groups continuously decreased, whereas the relative intensity of the second signal was found to increase, with a crossover between 30 and 50 GPa. Moreover, the total intensity was found to decrease significantly by a factor of 2 at 64 GPa compared to 8 GPa, indicating a dissociation of hydrogen atoms and reformation to a compound, possibly molecular hydrogen, which could not be observed in these experiments. Figure 4C summarizes the obtained signal intensities throughout the whole experiment. Additional investigations of other alkanes, for example, heptane or decane, would certainly serve to further illuminate this effect, but because the main focus of this study is to prove the feasibility of the method, we did not pursue this issue.

2D homonuclear or heteronuclear COSY is one of the most widely used 2D NMR experiments (62) because it deconvolutes overlapping NMR signals arising from spectroscopically nonequivalent sites, which are broadened by chemical shift anisotropies or other broadening mechanisms.

As a final proof of the usefulness of the presented novel resonator design in high-pressure anvil cells, it is imperative to investigate the inherent spectral resolution in a system with two or more observable proton signals. To this end, we have chosen to use thymine ($C_5H_6N_2O_2$), one of the four nucleobases of DNA, because it exhibits two relatively strong proton signals from methyl and methine groups, plus an additional signal of amide groups—all of which are reasonably well separated in frequency space.

A homonuclear COSY NMR spectrum at about 1 to 1.5 GPa in a pressure cell using Lenz lenses is shown in fig. S6. Three reasonably well separated proton signals stemming from all proton sites could be observed. Because of significant line broadenings and short coherence transfer mixing times, no cross-peaks were observed. The spectral resolution, given by the FWHM linewidth of the intense H^α signals, was found to be 3.7 ppm. This value is about twice as high as the FWHM linewidths found in Fig. 4, which possibly originates in hindered motional averaging of the thymine molecules because the D_2O solution is close to its crystallization point at this pressure. Nevertheless, although these linewidths are by far not as sharp as compared with observed signals in solution state NMR, it certainly allows the observation of several nonequivalent proton peaks within one compound. Furthermore, because most of the systems observable under pressure will eventually become solid, this spectral resolution can be considered more than optimal for most high-pressure solid-state NMR investigations.

DISCUSSION

This study introduces a novel way to implement NMR experiments in DACs using inductively coupled Lenz lenses, which allow an increased NMR sensitivity throughout the whole high-pressure experiment and significantly higher pressures compared to all former experimental approaches. The advantages of this setup compared to formerly used high-pressure NMR resonators are manifold.

First, Lenz lenses allow a significantly higher spin sensitivity, and thus excellent LOD in the order of 10^{12} spins$/\sqrt{Hz}$, which corresponds to a detectable volume of only 15 μm^3 within a bandwidth of 1 Hz of a water sample. These high sensitivities are ideal for applications suffering from highly limited sample volumes that barely fit in the limited space of a DAC. Moreover, because the sensitivity does not deteriorate with pressure, very high sensitivity NMR at 1 Mbar and beyond becomes possible, even more so as the RF B_1 field and hence the mass sensitivity can be further increased when the central hole of the lens is minimized.

Second, the Lenz lenses constitute the first quasi-2D RF resonators used for high-pressure applications, resulting in substantially higher possible pressures because the overall pressure cell setup is not altered significantly compared to microcoil setups, where small grooves in the metallic gasket are mandatory to avoid premature coil gasket short circuit. Last, this study also demonstrates that ^{1}H NMR is possible without the interference of spurious signals—typically originating from organic materials close to the resonator such as wire insulations or epoxy resins—which are prone to distort or completely mask the weak proton signal originating from within the sample chamber.
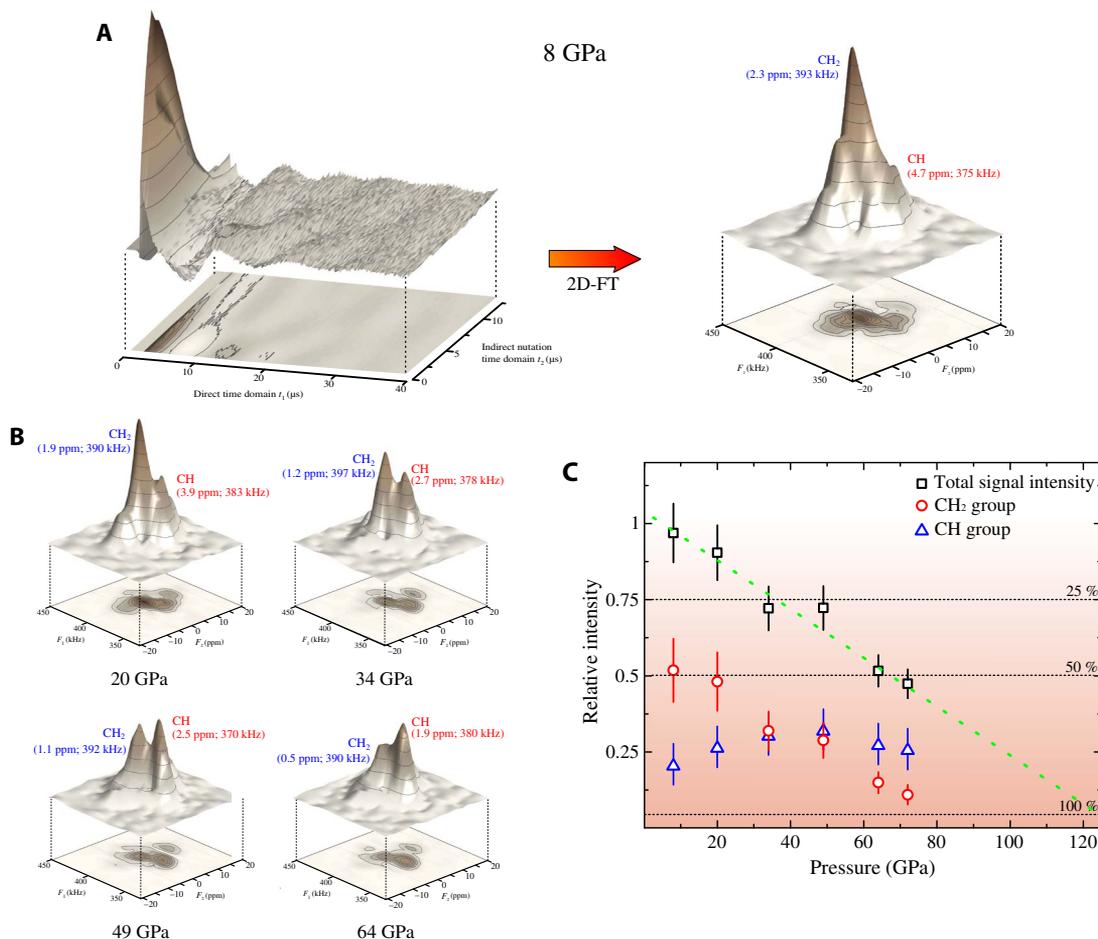
Fig. 4. 2D nutation spectroscopy experiments on paraffin oil up to 64 GPa. (**A**) In time domain, the obtained data consist of the direct dimension t_1 of the free induction decays (FIDs) that correlated with the indirect dimension t_2 defined by the incrementally increasing RF pulse lengths. Fourier transform (FT) in both dimensions yields the 2D nutation spectrum. (**B**) Comparison of obtained 2D nutation spectra of paraffin at pressures up to 64 GPa. All spectra are normalized relative to 8 GPa, thus evidencing a loss in total NMR signal intensity. (**C**) Summary of 2D intensities for both spectral species and the total intensity. The nutation spectra were acquired at 16-W pulse power.

In addition, it could be shown that more advanced 2D NMR methods can be easily used, yielding further information content, which would not be possible to access in 1D NMR experiments. This might be particularly advantageous when the 1D spectral resolution is limited to some parts per million, and signals from nonequivalent species overlap significantly, hampering data analysis.

Recently, some possible alternatives to Lenz lens resonators were introduced, namely, planar multiturn microcoils (*41*, *63*, *64*), pseudo-stripline resonators (*65*, *66*), or even the detection of NMR signals through nitrogen vacancies in a diamond matrix (*67*, *68*). Compared to these approaches, the presented NMR setup has some intriguing advantages. First, although the deformation of the lenses under pressure was shown to be well within acceptable limits and the overall shape remained intact, the structure of planar microcoils will most certainly be distorted significantly and electrical leads are eventually destroyed. Second, inductive coupling between excitation coil and lens circumvents the risk of short circuits of wires entering the high-pressure chamber, which typically limits the application of electrical transport or high-frequency measurements, such as de Haas–van Alphen measurements, to below 30 GPa. In this vein, stripline resonators would also be severely deformed and cut off at the edge of the diamond tips. These problems could be partially resolved by the application of bevelled

diamonds, which allow a somewhat safer passage of any electrical leads, but nonetheless, pressure remains limited to below 50 GPa. Third, concerning the possible application of negatively charged nitrogen vacancy centers in diamond, Doherty *et al.* (*69*) recently presented the first application of optically detected magnetic resonance (ODMR) in a DAC at pressures of up to 60 GPa, but because of internal strains under pressure, the transition energy of electrons was found to be significantly broadened, leading to extensively broadened ODMR spectra, which certainly prohibit high-resolution NMR using this technique.

The paramount significance of this new approach for high-pressure chemistry, physics, and mineralogy becomes obvious if the current state-of-the-art high-pressure NMR technique used to study liquid systems investigating proteins (*70*, *71*) is considered. This technique uses rather large RF resonators in an autoclave system, with sample volumes in the order of 10 to 100 μl, yielding sensitivities of about 10^{18} to 10^{19} spins/$\sqrt{\mathrm{Hz}}$ at considerably lower maximal pressures of less than 1 GPa (*70*, *72*). Therefore, the application of Lenz lenses in modern high-pressure vessels, yielding significantly higher sensitivities and allowing an observation of weak NMR signals stemming from ultrasmall samples, could lead to a widespread interest of NMR investigations of a plethora of new phenomena at considerably higher pressures than possible before.

MATERIALS AND METHODS
Cell preparation
All experiments were conducted with a pressure cell of type BX90 (*73*) made from nonmagnetic NiCrAl, which is known to generate pressures in the multi-megabar range (*74–76*). The diamond seats were made from nonmagnetic sintered cubic boron nitride and provided the necessary mechanical strength to support the diamonds under pressure.

For the first experiments, we chose to use a toroidal diamond indenter cell (TDIC) design, which was prepared as follows. Diamonds flattened to 250- and 800-μm culets were used, resulting in a buckled gasket after preindentation, enabling fragile coils to be positioned close to the 800-μm culet. The gasket was preindented to a thickness of 20 μm, and a 100-μm hole was cut in the flat indentation with an automated laser drilling system. Afterward, one side of the metallic rhenium gasket was sputter-coated with 2 μm of Al_2O_3 to avoid short circuiting between gasket and lens, and to prevent a complete closure of the slit of the lenses under pressure. In addition, under preindentation, the side of the 800-μm culeted anvil was found to be indented by about 10 to 20 μm, which provided a convenient sealing of the lens when liquid samples or pressure transmitting media are used. After preindentation, a small (100-μm-diameter and 10-μm-deep) cylindrical recess was cut in the culet of the 250-μm diamond anvil (see fig. S1) using a focused ion beam (FIB), increasing the total initial sample volume to about 230 pl. The internal pressure in the chamber was determined using the stress-dependent shift of the first-order Raman spectrum (*77*) at the center of the culet of the 250-μm diamond. The obtained Raman spectra up to 72 GPa are shown in fig. S2.

The internal pressure in the sample chamber was calculated using

$$P\,(\text{GPa}) \cong K_0 \frac{\Delta\nu}{\nu_0} \left(1 + \frac{1}{2} \left(K_0^{'} - 1 \right) \frac{\Delta\nu}{\nu_0} \right) \qquad (2)$$

where the diamond bulk modulus $K_0 = 547$ GPa and its pressure derivative $K_0^{'} = 3.75$, ν_0 denotes the ambient pressure first-order Raman band of the diamond edge located at $\nu_0 = 1333$ cm^{-1}, and $\Delta\nu$ is the induced pressure-dependent frequency shift measured at the center of the culet.

RF characterization of the resonator and test measurements
Setting up the resonator was done in two steps. At first, a small (1-mm-diameter) coil with three turns was made from 100-μm polytetrafluoroethylene-insulated copper wire and fixed on the pavilion of the 800-μm diamond anvil so that the culet is centered within the coil. The leads of the coil were soldered to copper tape, leading to the exterior of the pressure cell. In addition, a 15-pF nonmagnetic surface-mount device chip capacitor was soldered parallel and as close as possible to the coil onto the copper tape to close the resonator at a resonance frequency of 400.13 MHz, which corresponds to the nuclear Larmor frequency of hydrogen nuclei in a magnetic field of 9.4 T. Outside the cell, two variable glass capacitors were used for frequency fine tuning and impedance matching. The resonator was grounded over the pressure cell and the probe.

Second, the Lenz lens was manufactured from 5-μm-thick gold foil, cutting out the final geometry with a pulsed laser drilling machine. The lenses have an outer diameter of 600 μm, an inner diameter matching the diameter of the sample chamber, and a 30-μm-wide slit. After cutting, the lenses were carefully placed at the center of the 800-μm culet. The RF setup, including the Lenz lens before loading as well as the

corresponding return loss spectrum and a smith chart analysis of the resonator at 400 MHz, is shown in fig. S3. Almost ideal matching conditions of the excitation coil with a quality factor of 20 could be realized.

All NMR experiments were conducted at a proton Larmor frequency of 400.13 MHz; optimal pulse durations were determined using 2D pulse nutation experiments at every pressure step. All proton spectra were recorded with a 2 MHz receiver bandwidth. To evidence that the signal originated from the paraffin oil within the sample chamber—and not from the surroundings of the resonator—we conducted four measurements at similar experimental conditions: before loading, after loading of the paraffin oil in the resonator at 1 bar, after the pressure run at ambient conditions, and finally after opening and careful cleaning of the cell (see fig. S4). The corresponding proton spectra did not show any proton signals in the case when paraffin oil was absent from the center of the Lenz lens while exhibiting two almost identical intense ^{1}H NMR spectra at ambient conditions before and after compression. Thus, the observed signals must originate from the paraffin oil centered at the sample chamber. Spurious signals were not detected.

SNR$_t$ and LOD
Hoult and Richards (*36*) first comprehensively derived the time-domain SNR in an NMR experiment after the application of a single π/2 pulse, which was later refined by Peck *et al.* (*16*)

$$\text{SNR}_t = \frac{B_1}{i} \cdot \frac{\omega_0^2}{3\sqrt{2}k_B T} \cdot \frac{\kappa_0 V_s N_s \gamma_n \hbar^2 I(I+1)}{V_{\text{noise}}} \qquad (3)$$

where B_1 is the RF magnetic field generated by the resonator, i is the current, and ω_0 is the nuclear Larmor frequency of a particular nuclear spin with spin quantum number I and gyromagnetic ratio γ_n. V_s and N_s are the sample volume and the spin density of the sample, respectively. The thermal noise voltage V_{noise} is given by the Johnson-Nyquist expression (*78, 79*)

$$V_{\text{noise}} = \sqrt{4k_B T R_{\text{noise}} \Delta f} \qquad (4)$$

where the electric resistance R_{noise} is governed by Ohm's law corrected for limited RF penetration and Δf is the operating bandwidth of the NMR receiver.

Here, SNR$_t$ was obtained by comparing the maximal signal amplitude of the resulting FIDs in time domain extrapolated toward $t = 0$ (directly after the end of the exciting RF pulse) with the noise voltage spectral density of the detected signal in the white noise region.

The number of hydrogen spins that contribute to the obtained signals shown in fig. S4 and Fig. 2 was calculated given the total initial sample volume of 230 pl and the density of paraffin oil of 800 kg m^{-3}. The final time-domain LOD were calculated using Eq. 1.

The values for LOD$_t$ in the microcoil experiments were obtained by direct evaluation of SNR$_t$ from the original data (*22, 23*) as well as gauged from the published frequency domain spectra (*49*) and compared with the corresponding time-domain FIDs (*52*).

2D NMR experiments
For the 2D nutation experiments, a TDIC pressure cell, similar to that used for the 1D measurements, was prepared using the same experimental setup. The measurements were conducted at a Bruker Avance III 400 MHz system using a 9.3-T-wide bore magnet. The pulse lengths

were incremented in steps of 100 ns, ranging from 100 ns to 25.6 μs, yielding an indirect time-domain size of 256 points. For the ^{1}H-^{1}H COSY measurements, a solution of deuterated water and thymine was prepared in a mass ratio of roughly 1:10. The mixture was prepared within the sample cavity of the TDIC pressure cell, which was closed and pressurized rapidly to about 1 to 1.5 GPa within several seconds. After loading, excess liquid was removed and the cell was left overnight to allow all additional liquids to evaporate to avoid detection of spurious signals not stemming from within the sample cavity. The homonuclear COSY measurements were conducted at a magnetic field of 9.3 T, with 90° pulse lengths of 3 μs. The mixing times were kept short to suppress cross-peaks and to only observe the diagonal peak signals. The proton chemical shift was referenced relative to a tetramethylsilane-CDCl$_3$ solution placed in a small glass tube—sample volume of approximately 100 nl—which was fixed in a pressure cell between the diamond tips to mimic the same experimental conditions of a complete high-pressure assembly.

SUPPLEMENTARY MATERIALS

Supplementary material for this article is available at http://advances.sciencemag.org/cgi/content/full/3/12/eaao5242/DC1

fig. S1. SEM image of the 250-μm anvil with the 100-μm recess.
fig. S2. Raman spectra used for pressure determination.
fig. S3. RF characterisation of the resonator.
fig. S4. ^{1}H NMR spectra.
fig. S5. Magnetic field maps of the B_1 fields generated by a microcoil of four turns (400 μm in diameter and 100 μm in height, left) and of a flat Lenz lens made from a solid sheet of gold foil (right).
fig. S6. ^{1}H-^{1}H COSY spectrum of thymine in a pressure cell at pressures close to the pressure-induced freezing point of the D$_2$O solvent.
fig. S7. ^{1}H NMR spectra.
section S1. ^{1}H NMR on ice VII up to 17 GPa.

REFERENCES AND NOTES

1. D. M. Grant, R. K. Harris, *Encyclopedia of Nuclear Magnetic Resonance* (John Wiley & Sons, 2007).
2. R. R. Ernst, Zurich's contributions to 50 years development of Bruker. *Angew. Chem. Int. Ed.* **490**, 8310–8315 (2010).
3. E. R. Andrew, A historical review of NMR and its clinical applications. *Br. Med. Bull.* **40**, 115–119 (1984).
4. P. C. Lauterbur, Image formation by induced local interactions: Examples employing nuclear magnetic resonance. *Nature* **242**, 190–191 (1973).
5. P. Mansfield, Snapshot magnetic resonance imaging (Nobel lecture). *Angew. Chem.* **43**, 5456–5464 (2004).
6. R. Riek, S. Hornemann, G. Wider, M. Billeter, R. Glockshuber, K. Wüthrich, NMR structure of the mouse prion protein domain PrP(121–231). *Nature* **3820**, 180–182 (1996).
7. R Zahn, A Liu, T Lührs, R Riek, C von Schroetter, F. López García, M. Billeter, L. Calzolai, G. Wider, K. Wüthrich, NMR solution structure of the human prion protein. *Proc. Natl. Acad. Sci. U.S.A.* **970**, 145–150 (2000).
8. H. A. Scheidt, A. Sickert, T. Meier, N. Castellucci, C. Tomasini, D. Huster, The interaction of lipid modified pseudopeptides with lipid membranes. *Org. Biomol. Chem.* **90**, 6998–7006 (2011).
9. J. L. Yarger, K. H. Smith, R. A. Nieman, J. Diefenbacher, G. H. Wolf, B. T. Poe, P. F. McMillan, Al coordination changes in high-pressure aluminosilicate liquids. *Science* **270**, 1964–1967 (1995).
10. J. F. Stebbins, Dynamics and structure of silicate and oxide melts: Nuclear magnetic resonance studies, in *Structure, Dynamics and Properties of Silicate Melts*, J. F. Stebbins, P. F. McMillan. D. B. Dingwell, Eds. (Mineralogical Society of America, ed. 1, 1995), pp. 191–246.
11. A. Sharma, J. H. Scott, G. D. Cody, M. L. Fogel, R. M. Hazen, R. J. Hemley, W. T. Huntress, Microbial activity at gigapascal pressures. *Science* **295**, 1514–1516 (2002).
12. I. Daniel, P. Oger, R. Winter, Origins of life and biochemistry under high-pressure conditions. *Chem. Soc. Rev.* **35**, 858–875 (2006).
13. Q. Huang, K. N. Tran, J. M. Rodgers, D. H. Bartlett, R. J. Hemley, T. Ichiye, A molecular perspective on the limits of life: Enzymes under pressure. *Condens. Matter Phys.* **19**, 22801 (2016).
14. E. Fukushima, S. B. W. Roeder. *Experimental Pulse NMR—A Nuts and Bolts Approach* (Addison Wesley, ed. 1, 1981).
15. T. Meier, At its extremes: NMR at giga-pascal pressures. *Annu. Rep. NMR Spectrosc.* **93**, 10.1016/bs.arnmr.2017.08.004 (2018).
16. T. L. Peck, R. L. Magin, P. C. Lauterbur, Design and analysis of microcoils for NMR microscopy. *J. Magn. Reson. B* **108**, 114–124 (1995).
17. M. E. Lacey, R. Subramanian, D. L. Olson, A. G. Webb, J. V. Sweedler, High-resolution NMR spectroscopy of sample volumes from 1 nl to 10 μl. *Chem. Rev.* **99**, 3133–3152 (1999).
18. A. M. Wolters, D. A. Jayawickrama, J. V. Sweedler, Microscale NMR. *Curr. Opin. Chem. Biol.* **60**, 711–716 (2002).
19. K. Yamauchi, J. W. G. Janssen, A. P. M. Kentgens, Implementing solenoid microcoils for wide-line solid-state NMR. *J. Magn. Reson.* **167**, 87–96 (2004).
20. T. Suzuki, I. Yamauchi, Y. Shimizu, M. Itoh, N. Takeshita, C. Terakura, H. Takagi, Y. Tokura, T. Yamauchi, Y. Ueda, High-pressure V-51 NMR study of the magnetic phase diagram and metal-insulator transition in quasi-one-dimensional beta-Na0.33V2O5. *Phys. Rev. B* **79**, 081101 (2009).
21. T. Meier, T. Herzig, J. Haase, Moissanite anvil cell design for giga-pascal nuclear magnetic resonance. *Rev. Sci. Instrum.* **850**, 043903 (2014).
22. T. Meier, S. Reichardt, J. Haase, High-sensitivity NMR beyond 200,000 atmospheres of pressure. *J. Magn. Reson.* **257**, 39–44 (2015).
23. T. Meier, J. Haase, Anvil cell gasket design for high pressure nuclear magnetic resonance experiments beyond 30 GPa. *Rev. Sci. Instrum.* **86**, 123906 (2015).
24. T. Meier, J. Haase, High-sensitivity nuclear magnetic resonance at giga-pascal pressures: A new tool for probing electronic and chemical properties of condensed matter under extreme conditions. *J. Vis. Exp.* e52243 (2014).
25. U. Schwarz, A. Grzechnik, K. Syassen, I. Loa, M. Hanfland, Rubidium-IV: A high pressure phase with complex crystal structure. *Phys. Rev. Lett.* **83**, 4085–4088 (1999).
26. E. Bykova, L. Dubrovinsky, N. Dubrovinskaia, M. Bykov, C. McCammon, S. V. Ovsyannikov, H.-P. Liermann, I. Kupenko, A. I. Chumakov, R. Rüffer, M. Hanfland, V. Prakapenka, Structural complexity of simple Fe$_2$O$_3$ at high pressures and temperatures. *Nat. Commun.* **7**, 10661 (2016).
27. D. J. Frost, C. Liebske, F. Langenhorst, C. McCammon, R. G. Tronnes, D. C. Rubie, Experimental evidence for the existence of iron-rich metal in the Earth's lower mantle. *Nature* **428**, 409–412 (2004).
28. I. Kupenko, C. McCammon, R. Sinmyo, V. Cerantola, V. Potapkin, A. I. Chumakov, A. Kantor, R. Rüffer, L. Dubrovinsky, Oxidation state of the lower mantle: In situ observations of the iron electronic configuration in bridgmanite at extreme conditions. *Earth Planet. Sci. Lett.* **423**, 78–86 (2015).
29. A. Kurnosov, H. Marquardt, D. J. Frost, T. Boffa Ballaran, L. Ziberna, Evidence for a Fe^{3+}-rich pyrolitic lower mantle from (Al,Fe)-bearing bridgmanite elasticity data. *Nature* **543**, 543–546 (2017).
30. M. I. Eremets, I. A. Trojan, Conductive dense hydrogen. *Nat. Mater.* **10**, 927–931 (2011).
31. M. I. Eremets, I. A. Troyan, A. P. Drozdov, Low temperature phase diagram of hydrogen at pressures up to 380 GPa. A possible metallic phase at 360 GPa and 200 K. http://arxiv.org/abs/1601.04479 (2016).
32. P. Dalladay-Simpson, R. T. Howie, E. Gregoryanz, Evidence for a new phase of dense hydrogen above 325 gigapascals. *Nature* **529**, 63–67 (2016).
33. R. P. Dias, I. F. Silvera, Observation of the Wigner-Huntington transition to metallic hydrogen. *Science* eaal1579 (2017).
34. J. Schoenmaker, K. R. Pirota, J. C. Teixeira, Magnetic flux amplification by Lenz lenses. *Rev. Sci. Instrum.* **840**, 085120 (2013).
35. N. Spengler, P. T. While, M. V. Meissner, U. Wallrabe, J. G. Korvink, Magnetic Lenz lenses increase the limit-of-detection in nuclear magnetic resonance. http://arxiv.org/abs/1606.07044 (2016).
36. D. I. Hoult, R. E. Richards, The signal-to-noise ratio of the nuclear magnetic resonance experiment. *J. Magn. Reson.* **24**, 71–85 (1976).
37. D. I. Hoult, The principle of reciprocity in signal strength calculations—A mathematical guide. *Concepts Magn. Reson. Part A* **120**, 173–187 (2000).
38. D. I. Hoult, The principle of reciprocity. *J. Magn. Reson.* **213**, 344–346 (2011).
39. D. Sakellariou, G. Le Goff, J.-F. Jacquinot, High-resolution, high-sensitivity NMR of nanolitre anisotropic samples by coil spinning. *Nature* **447**, 694–697 (2007).
40. V. Badilita, B. Fassbender, K. Kratt, A. Wong, C. Bonhomme, D. Sakellariou, J. G. Korvink, U. Wallrabe, Microfabricated inserts for magic angle coil spinning (MACS) wireless NMR spectroscopy. *PLOS ONE* **7**, e42848 (2012).
41. H. Ryan, S.-H. Song, A. Zaß, J. Korvink, M. Utz, Contactless NMR spectroscopy on a chip. *Anal. Chem.* **84**, 3696–3702 (2012).
42. T. Okuchi, R. J. Hemley, H.-k. Mao, Radio frequency probe with improved sensitivity for diamond anvil cell nuclear magnetic resonance. *Rev. Sci. Instrum.* **76**, 026111 (2005).
43. J. W. Otto, J. K. Vassiliou, G. Frommeyer, Nonhydrostatic compression of elastically anisotropic polycrystals. I. Hydrostatic limits of 4:1 methanol-ethanol and paraffin oil. *Phys. Rev. B* **57**, 3253–3263 (1998).

44. N. Tateiwa, Y. Haga, Evaluations of pressure-transmitting media for cryogenic experiments with diamond anvil cell. *Rev. Sci. Instrum.* **800**, 123901 (2009).
45. N. Tateiwa, Y. Haga, Appropriate pressure-transmitting media for cryogenic experiment in the diamond anvil cell up to 10 GPa. *J. Phys. Conf. Ser.* **215**, 012178 (2010).
46. T. Okuchi, G. D. Cody, H.-k. Mao, R. J. Hemley, Hydrogen bonding and dynamics of methanol by high-pressure diamond-anvil cell NMR. *J. Chem. Phys.* **122**, 244509 (2005).
47. T. Okuchi, M. Takigawa, J. Shu, H.-k. Mao, R. J. Hemley, T. Yagi, Fast molecular transport in hydrogen hydrates by high-pressure diamond anvil cell NMR. *Phys. Rev. B* **750**, 144104 (2007).
48. T. Okuchi, Collision and diffusion dynamics of dense molecular hydrogen by diamond anvil cell nuclear magnetic resonance. *J. Phys. Chem. C* **116**, 2179–2182 (2011).
49. T. Meissner, S. K. Goh, J. Haase, M. Richter, K. Koepernik, H. Eschrig, Nuclear magnetic resonance at up to 10.1 GPa pressure detects an electronic topological transition in aluminum metal. *J. Phys. Condens. Matter* **26**, 015501 (2014).
50. P. J. M. van Bentum, J. W. G. Janssen, A. P. M. Kentgens, J. Bart, J. G. E. Gardeniers, Stripline probes for nuclear magnetic resonance. *J. Magn. Reson.* **189**, 104–113 (2007).
51. T. Meier, "High sensitivity nuclear magnetic resonance at extreme pressures," thesis, Leipzig University (2016).
52. T. Meissner, "Exploring nuclear magnetic resonance at the highest pressures," thesis, Leipzig University (2013).
53. M. G. G. Pravica, I. F. Silvera, Nuclear magnetic resonance in a diamond anvil cell at very high pressures. *Rev. Sci. Instrum.* **69**, 479–484 (1998).
54. M. G. Pravica, I. F. Silvera, NMR study of ortho-para conversion at high pressure in hydrogen. *Phys. Rev. Lett.* **81**, 4180–4183 (1998).
55. P. H. Sutter, A. S. Nowick, Ionic conductivity and time-dependent polarization in NaCl crystals. *J. Appl. Phys.* **34**, 734–746 (1963).
56. A. N. Babushkin, G. V. Babushkina, O. A. Ignatchenko, Electrical characteristics of dielectrics and semiconductors at high pressures in diamond anvil cell. *J. High Pressure School* **1**, 32–36 (1999).
57. Y. Volkova, A. N. Babushkin, Electrical characteristics of NaCl at frequencies of 1-100 kHz at superhigh pressures. Application of an impedance spectroscopy. *Def. Diff. Forum* **208–209**, 303–306 (2002).
58. A. Samoson, E. Lippmaa, 2D NMR nutation spectroscopy in solids. *J. Magn. Reson.* **79**, 255–268 (1988).
59. A. P. M. Kentgens, J. J. M. Lemmens, F. M. M. Geurts, W. S. Veeman, Two-dimensional solid-state nutation NMR of half-integer quadrupolar nuclei. *J. Magn. Reson.* **71**, 62–74 (1987).
60. P. P. Man, J. Klinowski, Quadrupole nutation ^{27}Al NMR studies of isomorphous substitution of aluminium in the framework of zeolite Y. *Chem. Phys. Lett.* **147**, 581–584 (1988).
61. P. P. Man, Investigation of the central line of ^{55}Mn in KMn0$_4$ by a two-dimensional NMR method. *J. Magn. Reson.* **90**, 78–90 (1986).
62. G. A. Morris, J. W. Emsley, *Multidimensional NMR Methods for the Solution State* (John Wiley & Sons, ed. 1, 2010).
63. J. Anders, P. SanGiorgio, G. Boero, A fully integrated IQ-receiver for NMR microscopy. *J. Magn. Reson.* **209**, 1–7 (2011).
64. J. Anders, G. Chiaramonte, P. SanGiorgio, G. Boero, A single-chip array of NMR receivers. *J. Magn. Reson.* **201**, 239–249 (2009).
65. J. Bart, A. J. Kolkman, A. J. Oosthoek-de Vries, K. Koch, P. J. Nieuwland, H. J. W. G. Janssen, J. van Bentum, K. A. M. Ampt, F. P. J. T. Rutjes, S. S. Wijmenga, H. Gardeniers, A. P. M. Kentgens, A microfluidic high-resolution NMR flow probe. *J. Am. Chem. Soc.* **131**, 5014–5015 (2009).
66. J. Bart, J. W. G. Janssen, P. J. M. van Bentum, A. P. M. Kentgens, J. G. E. Gardeniers, Optimization of stripline-based microfluidic chips for high-resolution NMR. *J. Magn. Reson.* **201**, 175–185 (2009).
67. N. Aslam, M. Pfender, P. Neumann, R. Reuter, A. Zappe, F. F. de Oliveira, A. Denisenko, H. Sumiya, S. Onoda, J. Wrachtrup, Nanoscale nuclear magnetic resonance with chemical resolution. *Science* **357**, 67–71 (2017).
68. J. Jeske, D. W. M. Lau, X. Vidal, L. P. Mcguinness, P. Reineck, B. C. Johnson, M. W. Doherty, J. C. McCallum, S. Onoda, F. Jelezko, T. Ohshima, T. Volz, J. H. Cole, B. C. Gibson, A. D. Greentree, Stimulated emission from nitrogen-vacancy centres in diamond. *Nat. Commun.* **8**, 14000 (2017).
69. M. W. Doherty, V. V. Struzhkin, D. A. Simpson, L. P. Mcguinness, Y. Meng, A. Stacey, T. J. Karle, R. J Hemley, N. B. Manson, L. C. L. Hollenberg, S. Prawer, Electronic properties and metrology applications of the diamond NV$^-$ center under pressure. **112**, 047601 (2014).
70. L. Ballard, J. Jonas, High-pressure NMR. *Annu. Rep. NMR Spectrosc.* **33**, 115–150 (1997).
71. W. Kremer, High-pressure NMR studies in proteins. *Annu. Rep. NMR Spectrosc.* **57**, 177–203 (2006).
72. M. R. Arnold, H. R. Kalbitzer, W. Kremer, High-sensitivity sapphire cells for high pressure NMR spectroscopy on proteins. *J. Magn. Reson.* **161**, 127–131 (2003).
73. I. Kantor, V. Prakapenka, A. Kantor, P. Dera, A. Kurnosov, S. Sinogeikin, N. Dubrovinskaia, L. Dubrovinsky, BX90: A new diamond anvil cell design for x-ray diffraction and optical measurements. *Rev. Sci. Instrum.* **83**, 125102 (2012).
74. L. Dubrovinsky, N. Dubrovinskaia, V. B. Prakapenka, A. M. Abakumov, Implementation of micro-ball nanodiamond anvils for high-pressure studies above 6 Mbar. *Nat. Commun.* **3**, 1163 (2012).
75. L. Dubrovinsky, N. Dubrovinskaia, E. Bykova, M. Bykov, V. Prakapenka, C. Prescher, K. Glazyrin, H.-P. Liermann, M. Hanfland, M. Ekholm, Q. Feng, L. V. Pourovskii, M. I. Katsnelson, J. M. Wills, I. A. Abrikosov, The most incompressible metal osmium at static pressures above 750 gigapascals. *Nature* **525**, 226–229 (2015).
76. N. Dubrovinskaia, L. Dubrovinsky, N. A. Solopova, A. M. Abakumov, S. Turner, M. Hanfland, E. Bykova, M. Bykov, C. Prescher, V. B. Prakapenka, S. Petitgirard, I. Chuvashova, B. Gasharova, Y.-L. Mathis, P. Ershov, I. Snigireva, A. Snigirev, Terapascal static pressure generation with ultrahigh yield strength nanodiamond. *Sci. Adv.* **2**, e1600341 (2016).
77. Y. Akahama, H. Kawamura, Pressure calibration of diamond anvil Raman gauge to 310 GPa. *J. Appl. Phys.* **100**, 043516 (2006).
78. J. B. Johnson, Thermal agitation of electricity in conductors. *Phys. Rev.* **32**, 97–109 (1928).
79. H. Nyquist, Thermal agitation of electric charge in conductors. *Phys. Rev.* **32**, 110–113 (1928).

ScienceAdvances

Magnetic flux tailoring through Lenz lenses for ultrasmall samples: A new pathway to high-pressure nuclear magnetic resonance

Thomas Meier, Nan Wang, Dario Mager, Jan G. Korvink, Sylvain Petitgirard and Leonid Dubrovinsky

ARTICLE TOOLS	http://advances.sciencemag.org/content/3/12/eaao5242
SUPPLEMENTARY MATERIALS	http://advances.sciencemag.org/content/suppl/2017/12/04/3.12.eaao5242.DC1
REFERENCES	This article cites 67 articles, 4 of which you can access for free http://advances.sciencemag.org/content/3/12/eaao5242#BIBL
PERMISSIONS	http://www.sciencemag.org/help/reprints-and-permissions

Use of this article is subject to the Terms of Service